Empirical detector model for simulated breast exams with a dedicated breast CT scanner

Antonio Sarno, Giovanni Mettivier, Koen Michielsen, Juan José Pautasso, Ioannis Sechopoulos, et al.

Antonio Sarno, Giovanni Mettivier, Koen Michielsen, Juan José Pautasso, Ioannis Sechopoulos, Paolo Russo, "Empirical detector model for simulated breast exams with a dedicated breast CT scanner," Proc. SPIE 12286, 16th International Workshop on Breast Imaging (IWBI2022), 1228605 (13 July 2022); doi: 10.1117/12.2624249

SPIE.

Event: Sixteenth International Workshop on Breast Imaging, 2022, Leuven, Belgium

Empirical detector model for simulated breast exams with a dedicated breast CT scanner

Antonio Sarno[1§*], Giovanni Mettivier[1], Koen Michielsen[2], Juan Jose Pautasso[2], Ioannis Sechopoulos[2,3,4] and Paolo Russo[1]

[1]Università degli Studi di Napoli "Federico II", Dipartimento di Fisica "Ettore Pancini" & INFN Sezione di Napoli, Naples, Italy
[2]Radboud University Medical Center, Department of Medical Imaging, Nijmegen, The Netherlands
[3]Technical Medical Centre, University of Twente, Enschede, The Netherlands
[4]Dutch Expert Center for Screening (LRCB), Nijmegen, The Netherlands
[§]presenter

*corresponding author: sarno@na.infn.it

ABSTRACT

This work proposes an empirical model for tuning spatial resolution and noise in simulated images in virtual clinical trials in x-ray breast imaging. In extending previous studies performed for direct conversion a-Se detectors used in digital mammography and digital breast tomosynthesis, this work introduces the model for the case of cone-beam computed tomography dedicated to the breast that uses a indirect conversion flat-panel detector. In the simulations, the detector is modeled as an absorbing layer whose material and thickness reflect those of the scintillator of the detector of a clinical scanner. The simulated images are then computed as a dose deposit map. The detector response curve, modulation transfer function (MTF) and noise power spectrum (NPS) were measured on a real detector. The same measurements were replicated *in-silico* for the simulated detector and scanner. The comparison of simulated and measured detector response curves permits to recover pixel values at the clinical scale. The difference between the simulated and measured MTFs permitted to introduce a linear filter for compensating simulated model simplification that determines a better spatial resolution in the simulated images with respect to real images. This filter presented a Gaussian shape in the Fourier domain with a standard deviation of 1.09 mm^{-1}, derived from those of the measured and simulated MTF curves, of 0.86 mm^{-1} and 1.41 mm^{-1}, respectively. Finally, the analysis of the NPS permits to compensate for noise characteristics due to the simulated model simplifications. The model applied to the simulated projection images produced MTF and normalized NPS in simulated 3D images, comparable to those obtained for the clinical scanner.

Keywords: Virtual clinical trials, CT dedicated to the breast, detector model.

1 INTRODUCTION

Virtual clinical trials in x-ray breast imaging conducted with Monte Carlo based platforms[1-4] require model simplifications which can impact the realism of the computed images. While, on the one hand, the realism of the digital patients can be obtained with sophisticated breast models – based on the knowledge of the anatomical structure of the organ[5] or derived from high resolution clinical images[6,7] – the computational model simplifications lead to neglecting some of the physical effects occurring in the detector and in the electronic chain[1-3]. Examples are the possibility of avoiding the tracking of

16th International Workshop on Breast Imaging (IWBI2022), edited by Hilde Bosmans, Nicholas Marshall, Chantal Van Ongeval, Proc. of SPIE Vol. 12286, 1228605
© 2022 SPIE · 0277-786X · doi: 10.1117/12.2624249

secondary electrons and hole-electron pairs or the simulation of optical photons for indirect detection flat-panel detector for reduction of model complexity and computational times. However, these simplifications may have some impact on the noise and spatial resolution of the computed images with a loss of realism. To address this topic, the AGATA project (INFN, Italy)[2,3] proposes to simulate the detector as an absorbing layer of defined material and thickness and tuning characteristics of the simulated images based on measured data from detector used in clinical scanners[8]. This work aims at extending the model elaborated for the a-Se direct conversion detectors of the Hologic Selenia Dimension DM/DBT scanner[8] to the characteristics of the detectors used for the Koning Corp cone-beam computed tomography scanner dedicated to the breast (breast CT, BCT).

2 MATERIAL AND METHODS

2.1 The Koning Corp. BCT detector

The Koning Corp. BCT scanner[9] embodies an indirect-conversion energy integrating detector with a CsI scintillator layer with a thickness of 0.6 mm. The native detector pixel pitch is 0.194 mm, but it works at 2 × 2 binning with an equivalent pixel pitch of 0.388 mm. The adopted spectra were generated with a 49 kV tube voltage and adopting a W/Al Anode/filter combination. The measured spectrum half value layer was 1.39 mm. 3D scan exams are performed with 300 projections acquired on a scan angle of 360°.

2.2 The AGATA simulation platform

In the AGATA Monte Carlo platform for virtual clinical trials in x-ray breast imaging[2,3], the detector of the simulated Koning BCT apparatus is modeled as a 0.6 mm CsI scintillator absorbing layer; detector images are computed as the 2D map of the radiation dose (mGy) deposited in the detector, adopting a sampling period of 0.388 mm. In the detector layer, de-excitation processes (fluorescence and Auger electrons generation) are simulated. Secondary electrons produced by Compton and photoelectric interactions are not tracked. Based on what used in the clinical Koning BCT apparatus, the x-ray beam was computed as suggested in Hernandez et al[10] by considering 49 kV tube voltage, W/Al anode/filter combination and a first half value layer of 1.39 mm Al.

2.3 Detector response curve and characteristics

Based on the linear and space invariant assumption of the detector response, the spatial resolution of the simulated images is tuned as follows:

$$I_R(x,y) = I_s(x,y) \otimes \mathrm{r(x,y)} \qquad (1)$$

where $\otimes$ is the 2D convolution operator, (x,y) are the spatial coordinates of the pixel on the detector plane, I_R is the processed image, I_S the simulated image, and $r(x,y)$ is a 2D Gaussian filter obtained by means of the inverse Fourier Transform of the R function that relates the measured modulation transfer function of the detector (MTF_M) to the simulated MTF (MTFs):

$$MTF_M(v,f) = MTF_s(v,f) \cdot \mathrm{R}(v,f) \qquad (2)$$

On the assumption of a Gaussian shape of the simulated and measured MTF curves[11], the $R(v,f)$ curve presents a Gaussian shape as well, whose standard deviation (σ_R) can be derived from those of the measured (σ_M) and simulated (σ_S) MTF as follows:

$$\sigma_R = \sqrt{\frac{\sigma_S^2 \cdot \sigma_M^2}{\sigma_S^2 - \sigma_M^2}} \qquad (3)$$

The MTF_M was evaluated via a tilted tungsten wire with a diameter of 50 μm placed in contact with the detector surface. Similarly, MTF_S was assessed by replicating the test *in-silico*. σ_M and σ_S were estimated by Gaussian fits of the measured and simulated MTF curves, respectively. Before the filtering operation of eq. (1), simulated pixel values (PVs) evaluated as pixel dose (mGy) are converted to realistic values by means of the measured and simulated detector response curves. These relate the image pixel values (expressed in mGy in the simulated images, and in arbitrary units in measured images) to the air kerma evaluated free-in-air at the scanner isocenter. In the clinical scanner, the air kerma was measured with a 6-cm^3 ion chamber (model 20X6-6, Radcal Corp, Monrovia, CA, USA) placed at the scanner isocenter. During the measurements, the gantry did not rotate. Similarly, the air kerma was computed in the *in-silico* AGATA platform from the

photon fluence incident on the cross-sectional area of the 6-cm^3 ion chamber[12] simulated at the scanner isocenter. For the computation of the detector response curve, pixel values were calculated as the average value in a region of interest (ROI) of 56 × 56 pixel at the detector chest-wall side, centered laterally. Noise characteristics were evaluated via the 1D noise power spectrum (NPS) as well as using the pixel standard deviation in a ROI, for exploring the need of including additional noise to *R*-tuned simulated images for reaching noise present in real projections. To evaluate the physical detector NPS (i.e., NPS of detector of the clinical apparatus), two flat-field projections were acquired for a fixed isocenter air kerma and the difference image was computed. The 2D NPS was then evaluated via the 2D FFT as suggested in Yang et al[13] and the 1D NPS computed as the average radial profile. The same test was replicated in-silico for modelling and comparison.

2.4 Simulated 3D images

Complete simulated scanning tests were performed by means the AGATA platform to evaluate the NPS and MTF in 3D computed images. NPS was evaluated as suggested in Yang et al[13] by means of the acquisition of images of a homogeneous PMMA cylindrical phantom with a diameter of 10 cm. Hence, the 2D NPS was evaluated from reconstructed axial slices (i.e., slices perpendicular to the gantry rotation axis) and 1D NPS was evaluated by radial averaging. To limit differences due to the absence of proper voxel values calibration, the normalized NPS (NNPS) was evaluated by dividing the 1D NPS by the square of the mean voxel value in a flat region of the reconstructed phantom. For MTF evaluation, a tungsten wire phantom with a diameter of 50 µm was used, placed at the isocenter of the simulated scanner and tilted by 2° with respect to the rotating axis, for evaluation of the pre-sampled point spread function (PSF) from several consecutive sample profiles acquired in radial direction[11]. The MTF in the radial direction was then evaluated via the FFT of the pre-sampled PSF. As used in the simulated Koning BCT scanner, 300 projections equally spaced over 360° scan angle were simulated. NNPS and MTF were also evaluated for the clinical scanner by means of the same tests as replicated *in-silico*. Both simulated and measured 3D images were computed from projections by means of the open-source Astra toolbox[14].

3 RESULTS

3.1 Detector model

Figure 1 reports the simulated and measured detector response curves (PV vs. air kerma at the scanner isocenter). In fig. 1a the response curve relates the simulated pixel dose (PD) to the air kerma at isocenter, and fig. 1b shows the PV of the Koning Corp BCT detector vs. the measured air kerma at the isocenter. Continuous-line curves are the linear fit curves, whose slope permits to convert PD to the PV of the clinical scanner as reported in eq. (4).

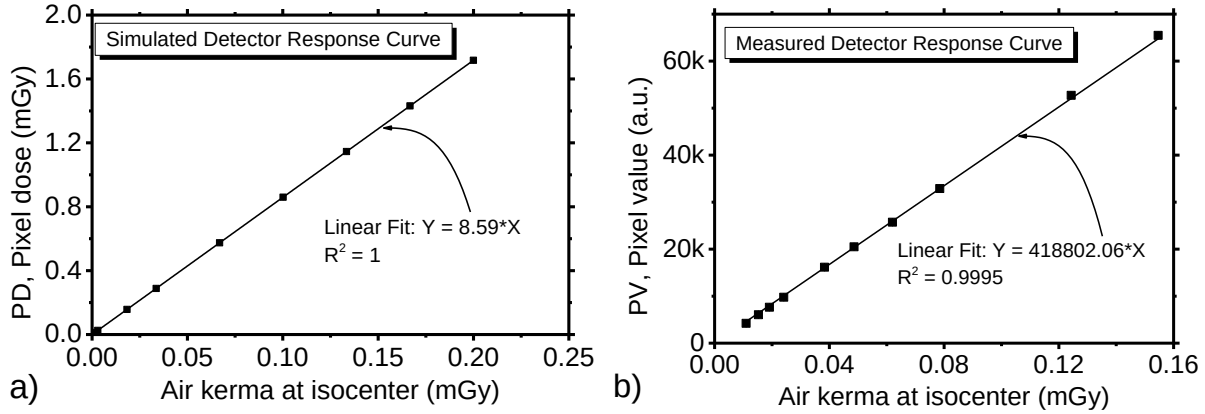

Figure 1. a) Simulated, and b) measured detector response curves. Continuous lines indicate linear curve fits, with intercept fixed to 0.

$$PV_s = PD \times \frac{418802.06}{8.59} \qquad (4)$$

Figure 2 shows the MTF_M and MTF_S as a function of spatial frequency, with the indication of the standard deviations of the Gaussian fit curves, σ_M and σ_S, estimated as 0.86 mm^{-1} and 1.41 mm^{-1}, respectively. The corresponding σ_R, evaluated as in eq. (3), was 1.09 mm^{-1}. The *R*-tuning in eq. (1) introduces a signal correlation over the detector and a reduction of the pixel standard deviation (pixel noise). This can be observed in fig. 3a, where the pixel standard deviation was evaluated in

both measured and simulated images in ROIs of 56 × 56 pixel, as well as in the simulated *R*-tuned images, for several exposure levels. The pixel noise of the simulated images - which resulted higher than the case of simulated images - reduces to values lower than the measured ones after the R-tuning. Figure 3b reports the residual noise ($\sigma_{residual}$) evaluated from the standard deviation of the measured images (σ_{meas}) and of the simulated R-tuned images (σ_{simR}), as follows [8]:

$$\sigma_{residual} = \sqrt{\sigma_{meas} - \sigma_{simR}} \qquad (5)$$

Here, $\sigma_{residual}$ is the standard deviation of noise to be added to the *R*-tuned simulated images to reach the noise level of the measured ones, under the assumption that the difference is due to sole additive Gaussian white noise (AWGN). Its value increases as the pixel value increases. To obtain a practical model of residual additive Gaussian noise needed to reach realistic noise values in simulated images, a non-linear monotone curve fit was calculated, as shown by the continuous curve in fig. 3b.

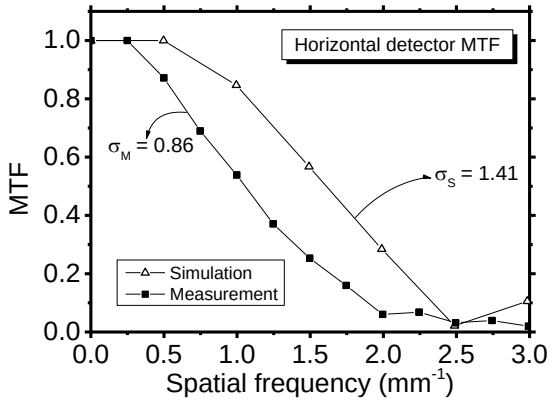

Figure 2. Measured and simulated MTF curves.

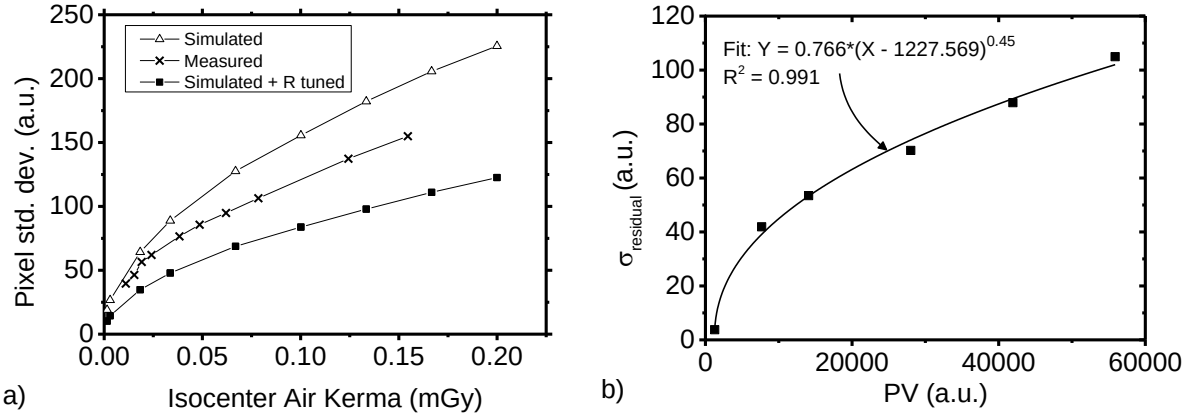

Figure 3. a) Pixel value standard deviation as a function of the air kerma at isocenter for measured flat field images, simulated flat-field images and simulated flat field images after the *R*-tuning. b) Pixel residual noise (standard deviation) between measured images and R-tuned simulated images as function of the pixel value.

Figure 4 shows the simulated and physical detector noise in the Fourier domain, by means of the 1D NPS. The noise of the simulated images is almost constant in the whole spatial frequency range, this being due to the little correlation between adjacent pixels in the in-silico detector model, caused mainly by the de-excitation processes. The *R*-tuning – used for reducing the spatial resolution of the simulated detector to that of the physical one – introduces a correlation in the noise spectra and a constant slope in the 1D NPS of the detector. The AWGN with standard deviation evaluated from the fitting curve in fig. 3b permitted to restore the noise level in the simulated images to that expected for the real detector. This AWGN contribution may be attributed to additional sources of noise (i.e., thermal noise, noise due to the light photons propagation and detection, etc.) that are not simulated but need to be included in the empirical model for simulated detector post processing.

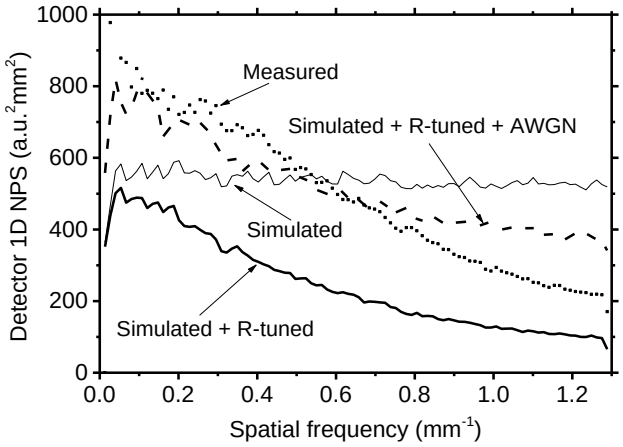

Figure 4. Measured, simulated, R-tuned and R-tuned AWGN included simulated detector 1D NPS. Air kerma at isocenter, 15.3 µGy.

3.2 3D noise and spatial resolution

Figure 5a shows measured and simulated MTF curves evaluated from 3D reconstructed images of the test tungsten wire at the scanner isocenter, at the chest-wall side and in the radial direction. The slight difference between the measured MTF in fig. 5a and that evaluated for the Koning scanner characterization reported in Sarno et al[15] may be attributed to the different reconstruction algorithm[16]. The effect of the *R*-tuning operated on the image projection is reflected also in 3D images, with a reduction of the MTF in simulated 3D images and a reduction of the differences with respect to the measured curve (fig. 5a). The effect of the *R*-tuning on the NNPS evaluated in 3D reconstructed images and reported in fig. 5b reflects that observed for NPS of the planar image projections. Hence, *R*-tuning, which is meant to modify the simulated images to present realistic spatial resolution, does also reduce and modify the spectral content of the noise. Figure 5b shows that NNPS is drastically reduced in simulated images by the *R*-tuning. However, AWGN noise suitably added to the manipulated projections by means of the curve model of fig. 3b, permits to recover the noise level present in measured images of the clinical Koning scanner.

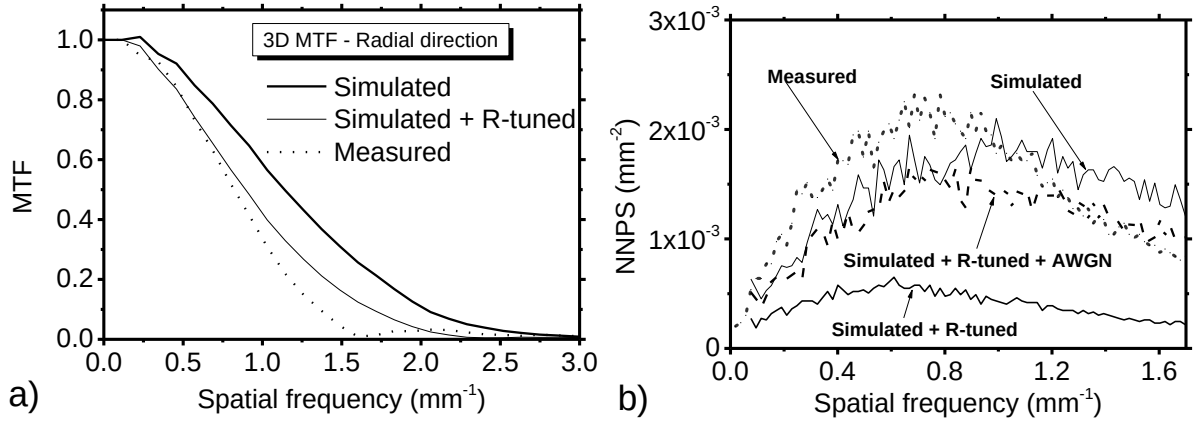

Figure 5. a) Measured, simulated, R-tuned simulated MTF from 3D reconstructed images in radial direction at the scanner isocenter. b) Measured, simulated, R-tuned and R-tuned AWGN included simulated 1D normalized NPS curves evaluated over the 3D PMMA phantom images. Air kerma at isocenter, 6.7 mGy, evaluated without the phantom in place.

4 CONCLUSIONS

This work proposes an empirical model for tuning noise and spatial resolution of Monte Carlo simulated images in x-ray breast imaging virtual clinical trials. It extends, to the case of a clinical BCT scanner, previous studies for direct detection a-Se detector used for DM/DBT scanners[8]. The method relies on the linear space invariant detector characteristics and

introduces a linear filter for compensating the differences in spatial resolution between simulated and real images. This filter is computed starting from differences of measured and simulated detector MTFs. Subsequently, a suitable noise model was employed for computing AWGN needed to reach noise power present in the images acquired via the physical clinical BCT scanner. The proposed approach does not include the gantry movement during the acquisition, which may affect the system spatial resolution: however, due to the pulsed x-ray source, this has a reduced impact on the image quality[15]. The proposed empirical method resulted appropriate to reproduce 3D simulated images with noise and spatial resolution of those acquired on the clinical scanner. Future tests will evaluate simulated lesion visibility also in comparison to tests on physical breast phantoms.

ACKNOWLEDGMENTS

This work was supported by the AGATA_GR5 project funded by INFN (Italy). Measurements were performed at the Radboud UMC (Nijmegen, The Netherlands).

REFERENCES

[1] Badal, A., Sharma, D., Graff, C. G., Zeng, R. and Badano, A., "Mammography and breast tomosynthesis simulator for virtual clinical trials," Comput. Phys. Commun. 261, 107779 (2021).

[2] Sarno, A., Mettivier, G., di Franco, F., Paternò, G., Taibi, A., Cardarelli, P., et al, "Advanced Monte Carlo application for in-silico clinical trials in x-ray breast imaging," 15th International Workshop on Breast Imaging (IWBI2020). Vol. 11513 (2020).

[3] di Franco, F., Sarno, A., Mettivier, G., Hernandez, A. M., Bliznakova, K., Boone, J. M. and Russo, P., "GEANT4 Monte Carlo simulations for virtual clinical trials in breast X-ray imaging: Proof of concept," Phys. Med. 74,133-142 (2020).

[4] Mettivier, G., Sarno, A., Lai, Y., Golosio, B., Fanti, V., Italiano, M. E. et al, "Virtual clinical trials in 2D and 3D x-ray breast imaging and dosimetry: Comparison of CPU-based and GPU-based Monte Carlo codes," Cancers 14(4),1027 (2022).

[5] Ikejimba, L. C., Graff, C. G., Rosenthal, S., Badal, A., Ghammraoui, B., Lo, J. Y. and Glick, S. J., "A novel physical anthropomorphic breast phantom for 2D and 3D x-ray imaging," Med. Phys. 44, 407-416 (2017).

[6] Sarno, A., Mettivier, G., di Franco, F., Varallo, A., Bliznakova, K., Hernandez, A. M. et al, "Dataset of patient-derived digital breast phantoms for in-silico studies in breast computed tomography, digital breast tomosynthesis and digital mammography," Med. Phys. 48, 2682-2693 (2021).

[7] Bliznakova, K., Dukov, N., Feradov, F., Gospodinova, G., Bliznakov, Z., Russo, P. et al, "Development of breast lesions models database," Phys. Med. 64, 293-303 (2019).

[8] Sarno A., Tucciariello, R. M., Fantacci, M. E., Traino, A. C., Mettivier, G., Valero, C., Stasi, M. and Russo P., "A Model for a Linear a-Se Detector in Simulated X-Ray Breast Imaging with Monte Carlo Software," In: 2021 IEEE Nuclear Science Symposium, Medical Imaging Conference and Room-Temperature Semiconductor Detector Workshop (NSS/MIC/RTSD). IEEE (2021).

[9] Sechopoulos, I., Feng, S. S. J. and D'Orsi, C. J., "Dosimetric characterization of a dedicated breast computed tomography clinical prototype," Med. Phys. 37, 4110-4120 (2010).

[10] Hernandez, A. M., Seibert, J. A., Nosratieh, A. and Boone, J. M., "Generation and analysis of clinically relevant breast imaging x-ray spectra," Med. Phys. 44, 2148-2160 (2017).

[11] Sarno, A., Mettivier, G., Di Lillo, F., Cesarelli, M., Bifulco, P. and Russo, P., "Cone-beam micro computed tomography dedicated to the breast," Med. Eng. Phys. 38, 1449-1457 (2016).

[12] Sarno, A., Mettivier, G. and Russo, P., "Air kerma calculation in Monte Carlo simulations for deriving normalized glandular dose coefficients in mammography," Phys. Med. Biol. 62, N337 (2016).

[13] Yang, K., Kwan, A. L., Huang, S. Y., Packard, N. J. and Boone, J. M., "Noise power properties of a cone-beam CT system for breast cancer detection," Med. Phys. 35, 5317-5327 (2008).

[14] Van Aarle, W., Palenstijn, W. J., Cant, J., Janssens, E., Bleichrodt, F., Dabravolski, A. et al, "Fast and flexible X-ray tomography using the ASTRA toolbox," Opt. express 24, 25129-25147 (2016).

[15] Sarno, A., Mettivier, G., Michielsen, K., Pautasso, J. J., Sechopoulos, I. and Russo P., "Noise and spatial resolution characteristics of a clinical Computed Tomography scanner dedicated to the breast," 16th International Workshop on Breast Imaging (IWBI2022).

[16] Betancourt-Benitez, R., Ning, R., Conover, D. L. and Liu, S., "Composite modulation transfer function evaluation of a cone beam computed tomography breast imaging system," Opt. Engineering 48, 117002 (2009).